Feasibility of unsupervised clustering method for two-phase flow regime classification using wire-mesh sensor under inclined air-water condition

Taehwi Kim^a, Hyukjae Ko^a, Hyoung Kyu Cho^a*

^aDept. of nuclear engineering, Seoul National Univ., 1 Gwanak-ro, Gwanak-gu, Seoul 08826

*Corresponding author: chohk@snu.ac.kr

*Keywords: Flow regime, Deep-clustering, Wire-mesh sensor, Inclined channel

1. Introduction

Floating nuclear power plant (FNPP) is gaining increasing attention due to its deployment flexibility. Operating under oceanic conditions where the system may experience inclination or rolling, its two-phase flow behavior is expected to be different from that of land-based reactors. In terms of flow regime, which is useful for predicting two-phase flow, for instance, MARS-KS [1] adopts a simplified approach based on vertical and horizontal flow regime map. This simplification highlights the necessity for more accurate flow regime maps under inclined conditions.

However, the development of flow regime map applicable for various geometric and flow conditions is challenging. Many previous studies relied on visual classification [2], an inherently subjective method, or relied on mechanistic models [3]. Mechanistic models provide a general framework, and the use of dimensionless numbers extends their applicability beyond specific geometric or operating conditions. However, they often group different flow regimes into a single intermittent flow, which limits their accuracy in representing transitional behaviors.

More recently, machine learning and deep learning have emerged as tools to overcome these limitations [4]. To ensure objectiveness and address the lack of robust criteria for inclined flows, unsupervised clustering can offer a promising alternative. Therefore, this study aims to assess the applicability of an unsupervised clustering method to flow regime classification using a database generated from wire-mesh sensor measurement of airwater flow under inclined condition.

2. Experimental apparatus

2.1 Experimental setup and conditions

The schematic diagram of the air-water flow experimental loop used in this study is shown in Fig. 1. The liquid goes through a reservoir, pump, flow meter and into the test section. The liquid flow rate is controlled by adjusting pump revolution speed and valve.

Air is supplied from a compressor, passes through a pressure regulator, rotameter, and then injected into the test section through a porous medium. The air flow rate was controlled by control valve attached to rotameter.

The acrylic test section with the channel diameter of 13 mm was used allowing simultaneous acquisition of high-speed camera (HSC) record and WMS data. Additionally, to capture side and top views of the channel, a mirror was also attached to the test section along with two backlights, providing sufficient light for each view.

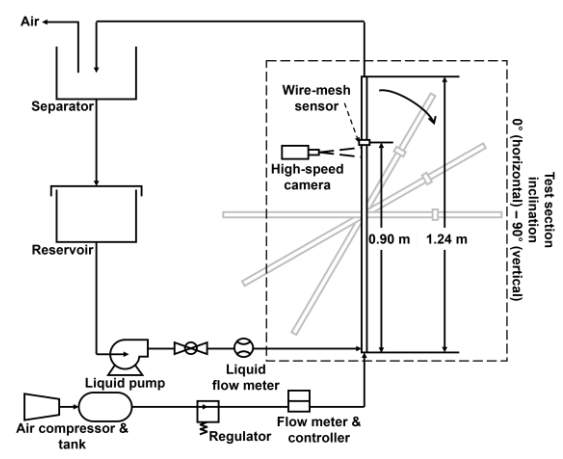


Figure 1. Schematic diagram of the experimental setup

Experiments were conducted under various inclination angles from 90° (vertical) to 0° (horizontal). In this study, assessment focusing on inclination angles 90° , 60° , 45° was conducted.

Table I: Experimental conditions

Superficial gas velocity	0.001 m/s - 2.51 m/s
Superficial liquid velocity	0.42 m/s - 1.26 m/s
Inclination (0°: horizontal)	$0^{\circ}-90^{\circ}$

2.2 Wire-mesh sensor

In this study, wire-mesh sensor was used to measure the local instantaneous conductivity of the two-phase mixture [5]. WMS is characterized by its ability to measure the void fraction distribution inside the channel.

WMS manufactured from HZDR (Helmholtz-Zentrum Dresden-Rossendorf) was used. Measuring plane consisting of transmitter-receiver wire array pair is comprised of 12×12 mesh configuration (1.083 mm pitch). Also, sensor used in this study has two measuring planes being 10 mm apart in axial direction, thereby enabling the measurement of gas phase velocity. Although WMS is capable of measuring at up to 10,000

fps, the measurements in this study were performed at 5,120 fps, sufficient for capturing 1 mm size bubbles moving at approximately $v_g = 1.2$ m/s at least four frames.

3. Visual identification

Three distinct flow regimes were identified from HSC videos: bubbly, slug, churn. In bubbly flow, distorted spherical bubbles appear, whereas slug flow is characterized by Taylor bubbles occupying the entire channel cross-section with liquid slugs containing many small bubbles. Churn flow exhibits irregular-shaped gas structures [6]. Additionally, cap-bubbly and developing slug flow where the gas units were not long enough to be identified as Taylor bubbles or hemispherical and cylindrical parts were not fully developed were observed between bubbly and slug flow. These structures could not be clearly categorized as either bubbly or slug and therefore intermediate regime was introduced. Fig. 2 shows representative images of the four regimes.

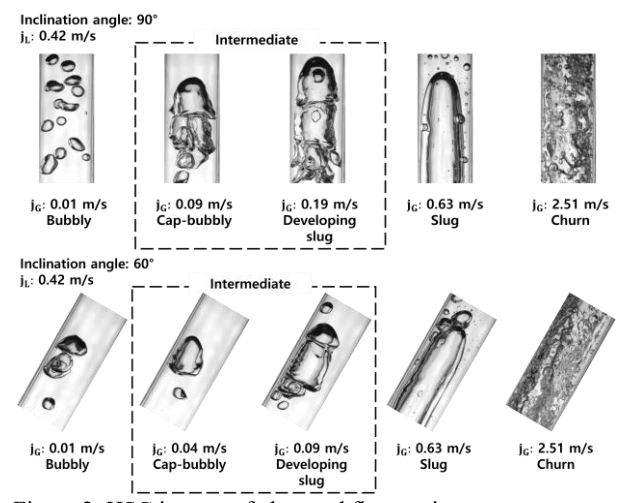


Figure 2. HSC images of observed flow regimes

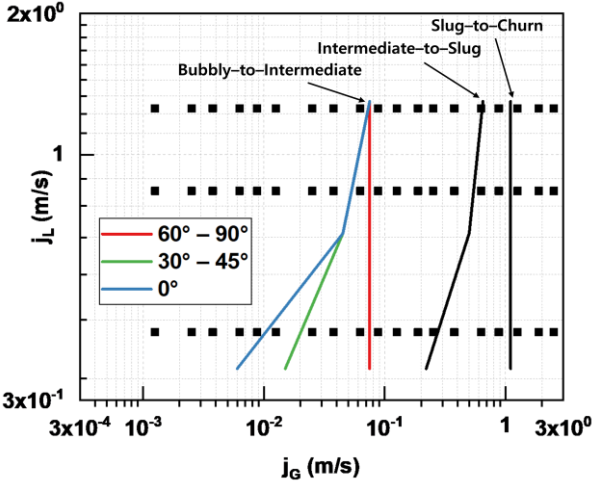


Figure 3. Visually identified flow regime transition

Fig. 3 illustrates visual identification result, where the lines indicate approximate regime boundaries. The bubbly-to-intermediate transition appeared around $j_G = 0.06-0.09$ m/s for $90^{\circ}-60^{\circ}$ but shifted to lower j_G with decreasing j_L at smaller inclinations, suggesting buoyancy-driven coalescence. The intermediate-to-slug transition occurred at lower j_G with decreasing j_L , likely due to reduced turbulence but showed little dependence on inclination. The slug-to-churn transition was seen near $j_G = 1.26$ m/s, regardless of inclination or j_L .

In this study, the test section had a smaller inner diameter (13 mm) and a shorter L/D ratio (70) than comparable studies (inner diameter > 25 mm, L/D ratio = 100-150). Many studies included cap-bubbly in bubbly flow, but the exact visual transition boundary between bubbly (including cap-bubbly)-to-slug was unclear under present conditions. Moreover, high j_L and j_G conditions under inclined geometries hinder visual identification due to numerous small bubbles surrounding the gas core.

Thus, visual or mechanistic approaches cannot ensure robust classification. Under such conditions, applying unsupervised clustering algorithms could provide a robust, and objective means of flow regime identification.

4. Application of unsupervised clustering method

4.1 Data preprocessing

Initially, WMS raw data representing instantaneous local fluid conductance was converted to void fraction by assuming a linear relationship between them. The gas phase velocity was then estimated by cross-correlating upstream and downstream sensor signals, which is used to transform the time axis into a physical length axis.

From the reconstructed dataset, two representative views were extracted: side-view and top-view. These 2D void fraction matrices were concatenated with zero padding so that each sample contained both perspectives of the flow. The final dataset had a shape of (27, 300), yielding a total of 143,736 examples.

This approach enables the construction of image-like datasets similar to HSC. However, it directly captures internal flow structures inside the core, and its image-like nature also suits it well for applying clustering methods originated from the computer vision field.

4.2 Clustering algorithm

The deep-clustering algorithm used in this study is 'Deep Embedded Clustering' (DEC) developed by J. Xie [7]. Currently, numerous deep clustering algorithms have been announced and continue to be advanced. However, this study adopts DEC for unsupervised clustering method considering it offers easier applicability and represents a pioneering deep clustering method that simultaneously optimizes representation learning and clustering. It has also served as a research

milestone with many subsequent variants developed from it.

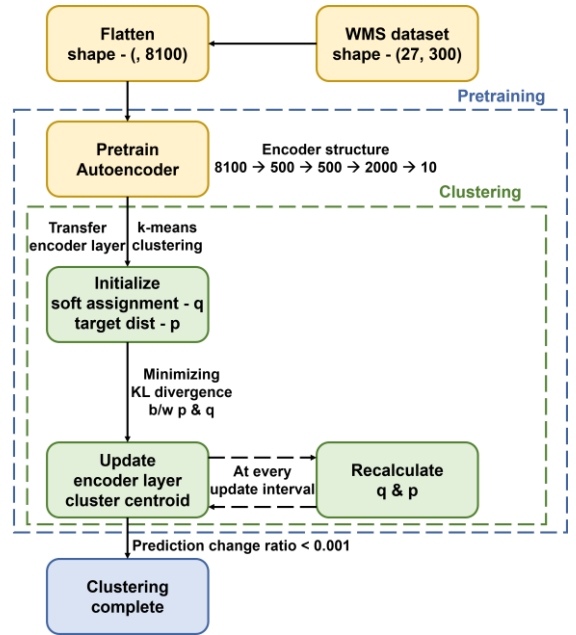


Figure 4. The overall pipeline of the DEC algorithm

DEC first trains a deep autoencoder to map the 8100dimensional input into a 10-dimensional latent space, where initial cluster centroids are obtained by k-means. Each embedded example is assigned to clusters with a soft probability, according to their similarity to the cluster centroids. To refine clustering, an auxiliary target distribution is derived from these assignments to emphasize confident samples and balance centroid contributions. The encoder and centroids are iteratively updated by minimizing the Kullback-Leibler divergence between the soft assignment and the target distribution, progressively improving representation and clustering until convergence.

In this study, to improve the convergence of the algorithm, batch-normalization layers were inserted between autoencoder layers. Batch normalization can mitigate the internal covariate shift, where the data distribution changes across batches causes instability. Batch-normalization parameters were fixed during the clustering phase to prevent drift in feature statistics. The process was terminated when convergence criterion is satisfied three times consecutively to ensure the reliability of the clustering result.

4.3 Classification using the DEC algorithm

The entire set of experimental results were classified into four clusters using the DEC. Fig. 5 shows results of clustering algorithm compared to visual identification and mechanistic model proposed by Barnea [3]. Unlike Fig. 3, the black lines correspond to visually determined flow regime boundaries for each inclination angle. The clustering result showed similar results to the visual classification capturing overall trends. At 90°, the mechanistic model predicted the intermediate-to-slug transition reasonably well, but under inclined conditions

it categorized most regions as intermittent, inconsistent with visual classification. It is notable that the algorithm could distinguish internal sub-regimes such as slug and churn like those identified by visual classification.

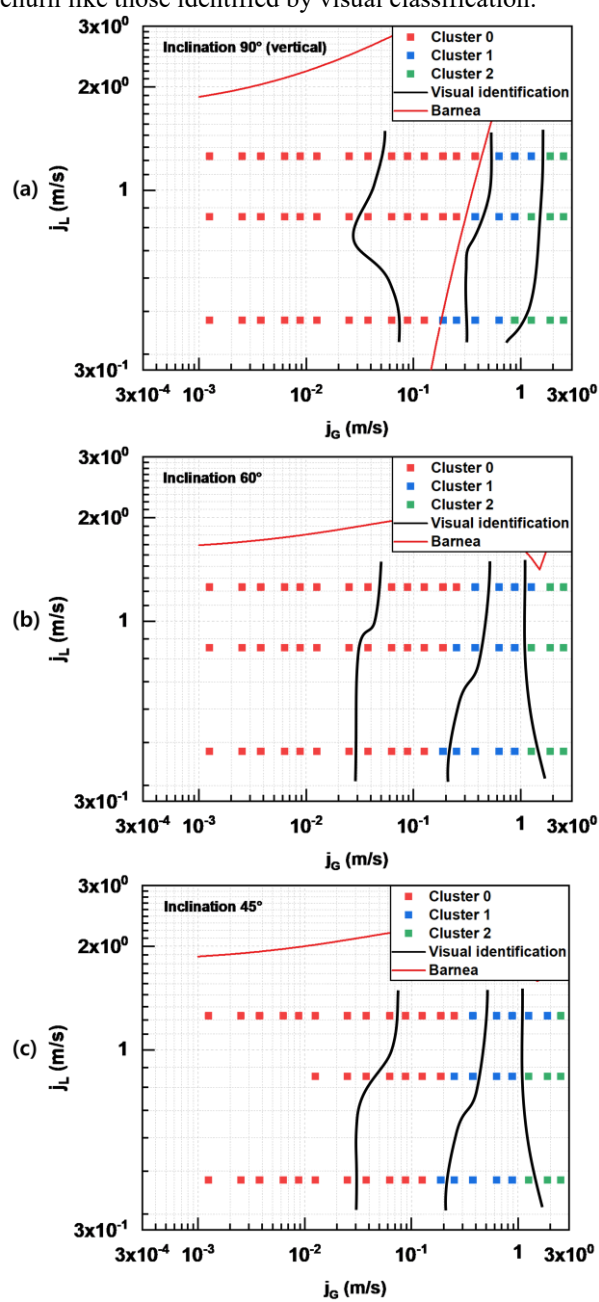


Figure 5. Results of clustering algorithm (solid symbol: experimental conditions, colors: cluster numbers classified by DEC) against visualization (black line) and mechanistic model (red line) proposed by Barnea [3] – inclination angle at (a): 90°, (b): 60°, (c): 45°

The algorithm was expected to capture not only the extent to which the gas phase occupies the examples, but also how that gas phase is spatially distributed, and this expectation was met. Fig. 6 presents clustering results together with WMS examples and HSC images near the slug-to-churn transition. Images (b), visually identified as slug, exhibit mean void fraction computed comparable to Case (c) than to Case (a). Despite this, the algorithm distinguished Case (b–c) based on spatial

distribution, assigning Case (b) to Cluster–1 and Case (c) to Cluster–2. These results demonstrate the potential of unsupervised clustering approach.

On the other hand, The DEC algorithm classified the entire set of experimental results into general categories (bubbly–slug–churn), rather than following the categories (bubbly–intermediate–slug–churn) used in visual identification. This was mainly because bubbly and intermediate flows overlapped in the latent space, making them difficult to separate.

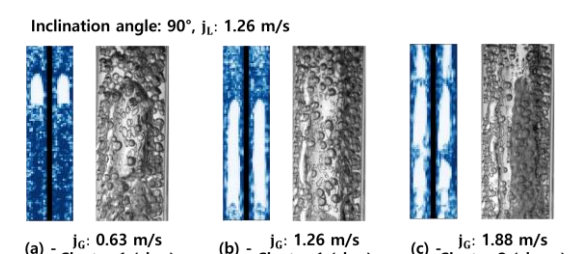


Figure 6. Comparison of HSC images and WMS dataset (only presented (27, 100) from total (27, 300)) between slug and churn flow

void fraction: 0.37

void fraction: 0.43

void fraction: 0.23

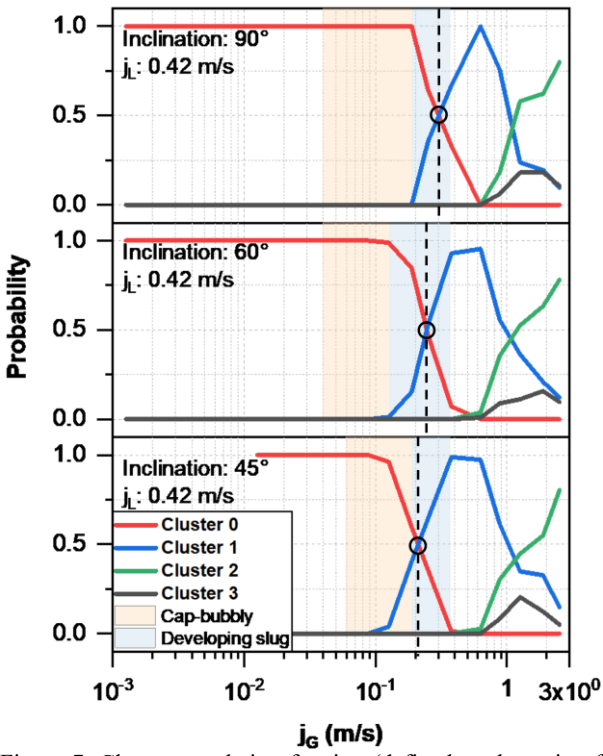


Figure 7. Cluster population fraction (defined as the ratio of examples assigned to each cluster to total examples)

Nevertheless, analysis of cluster assignment probability reveals useful insights into transitional behaviors. Fig. 7 shows the probability associated with Cluster–1 begins to increase from the latter part of the bubbly region where cap-bubbly can be expected to the onset of the developing slug. This indicates that a gradual bubbly-to-slug transition occurs within the intermediate regime, which cannot be observed in

discrete results such as those shown in Fig. 5. Conventional flow regime maps typically use lines to suggest that transitions between regimes occur discretely at specific points. In contrast, probability-based analysis could enable the boundaries to be represented as fuzzy bands. Furthermore, the crossing point of the probabilities corresponding to Cluster–0 and Cluster–1 (the transition point from Cluster–0 to Cluster–1) shifts to lower j_G values as the inclination angle decreases. This subtle transition, which cannot be clearly captured by visual identification due to human subjectiveness, can thus be objectively identified.

5. Conclusions

In this study, air—water two-phase flow experiments were conducted in a channel with various inclination angles using a wire-mesh sensor (WMS). Visual identification of flow regimes was performed, but its inherent subjectiveness and the ambiguity of regime boundaries, particularly between bubbly and slug flow, limited its reliability.

To address these limitations, an unsupervised clustering method was introduced. The algorithm successfully captured overall regime trends under inclined conditions, where mechanistic models did not make reliable predictions. Moreover, the probability-based analysis highlighted the extended applicability of unsupervised clustering method: instead of discrete boundaries, gradual flow regime transition was identified. This also enabled the detection of subtle transitions that conventional approaches could not resolve.

In summary, the unsupervised clustering combined with probability-based analysis can provide an objective and informative framework for flow regime classification in inclined channels, complementing both visual identification and mechanistic models.

REFERENCES

- [1] KAERI, MARS Code Manual, KAERI/TR-3872/2009, 2009.
- [2] G. F. Hewitt, D. N. Roberts, Studies of two-phase flow patterns by simultaneous X-ray and flash photography, AERE-M 2159, 1969.
- [3] D. Barnea, A unified model for predicting flow-pattern transitions for the whole range of pipe inclinations, International Journal of Multiphase Flow, Vol.13, pp.1-12, 1987.
- [4] Z. Huang, et al., Prediction of two-phase flow patterns based on machine learning, Nuclear Engineering and Design, Vol.421, 2024.
- [5] H.-M. Prasser, et al., A new electrode-mesh tomograph for gas-liquid flows, Flow measurement and Instrumentation, Vol.9, pp. 111-119, 1998.
- [6] S. Ghiaasiaan, Two-phase flow, boiling, and condensation, Cambridge University Press, 2011. pp.136-137.
- [7] J. Xie, et al., Unsupervised deep embedding for clustering analysis, Proceedings of the Machine Learning Research, Vol. 48, pp. 478-487, 2016.